

Radio-photoluminescence in Ag-doped Na–Al Borate Glass

Hiroki Kawamoto,* Yutaka Fujimoto, and Keisuke Asai

Department of Applied Chemistry, Graduate School of Engineering, Tohoku University,
6-6-07, Aoba, Aramaki, Aoba-ku, Sendai, Miyagi 980-8579, Japan

(Received October 30, 2023; accepted January 22, 2024)

Keywords: radio-photoluminescence, dosimeter, valence change of Ag, clustering of Ag, borate glass

In this paper, we report on the radio-photoluminescence (RPL) properties and RPL center formation mechanism in Ag-doped Na–Al borate glass (BG:Ag). In BG:Ag, broad emission bands at 550–800 and 450–800 nm with excitation wavelengths at 320 and 360 nm appeared after X-ray irradiation, respectively. The electron spin resonance (ESR) signal intensity of Ag^{2+} and Ag_2^+ increased with absorption dose. These results suggest that BG:Ag exhibits RPL from Ag^{2+} and Ag_2^+ . Furthermore, RPL emission bands and the ESR signals of Ag^{2+} and Ag_2^+ disappeared after heating at 773 K for 1 h. These results indicate that RPL centers can be eliminated by heating and that BG:Ag is a candidate reusable RPL material. On the basis of the variation of the ESR spectra with time from immediately after irradiation, we assumed the following RPL center formation mechanism. First, electron–hole pairs are generated by ionizing radiation. Some of the electrons are trapped at Ag^+ and form Ag^0 . Subsequently, Ag_2^+ ions are formed by the association of Ag^+ and Ag^0 . On the other hand, holes are trapped at the boron–oxygen network to form a boron oxygen hole center (BOHC). Subsequently, the trapped holes transfer to Ag^+ from BOHC and form Ag^{2+} .

1. Introduction

Radio-photoluminescence (RPL)^(1,2) is an emission phenomenon induced by the photoexcitation of luminescence centers (RPL centers) formed by irradiation with ionizing radiation, such as X-rays or gamma rays. Because the RPL intensity increases with absorption dose, RPL is applied to luminescent-type dosimeters. Similar phenomena applied in luminescent-type dosimeters include thermoluminescence^(3,4) (TL) and optically stimulated luminescence (OSL).⁽⁵⁾ In TL and OSL, electrons and holes formed by ionizing radiation are trapped separately at different sites, and the number of trapped electrons and holes corresponds to the amount of cumulative dose. Subsequently, trapped electrons and holes recombine to induce TL or OSL after excitation by heat or light, respectively.^(6,7) Trapped electrons and holes, in other words, information of cumulative dose, are lost by reading the absorption dose. In contrast, in an RPL process, electrons and holes formed by ionizing radiation are confined at trapping centers to form RPL centers. In RPL, the number of RPL centers corresponds to the amount of cumulative

*Corresponding author: e-mail: hiroki.kawamoto.e7@tohoku.ac.jp
<https://doi.org/10.18494/SAM4766>

dose. RPL is caused by the radiative transition of RPL centers by photoexcitation. In other words, an RPL process does not involve the recombination of electron–hole pairs formed by ionizing radiation, and the number of RPL centers does not change after emission. In addition, RPL has some unique characteristics such as high stability of RPL centers at room temperature and restoration of initial state by heating. Because of these characteristics, the absorption dose can be read and measured repeatedly using RPL dosimeters. Hence, RPL dosimeters are widely used in applications such as personal use,⁽⁸⁾ environmental monitoring,^(9–11) medical dosimetry,⁽¹²⁾ and dose imaging.^(13–16)

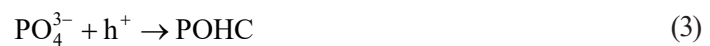
Previous researchers have reported some RPL materials⁽¹⁷⁾ such as Ag-doped phosphate glass,⁽¹⁸⁾ Ag-doped alkali halide,⁽¹⁹⁾ Ag-doped SrF₂,⁽²⁰⁾ Sm-doped CsBr,⁽²¹⁾ Sm-doped CaSO₄,⁽²²⁾ Eu-doped CaF₂,⁽²³⁾ Eu-doped CaSO₄,⁽²⁴⁾ and nondoped CaF₂.⁽²⁵⁾ Among these materials, Ag-doped phosphate glass is the most famous RPL material because this glass has been used in personal dosimeters sold as “glass badges” since the 1960s.⁽²⁶⁾ In Ag-doped phosphate glasses, Ag⁰, Ag²⁺, and Ag₂⁺ are attributed to be RPL centers.^(26–28) In addition, recently, high-order molecular silver clusters Ag_mⁿ⁺ formed in the high dose range have also been attributed to be RPL centers.⁽²⁹⁾ According to previous reports,^(26–30) the RPL center formation mechanism is as follows. First, electrons and holes are generated by ionizing radiation. Some of the electrons are trapped at Ag⁺ and form Ag⁰.



Subsequently, Ag₂⁺ ions are formed by the association of Ag⁺ and Ag⁰ via the diffusion of Ag⁺.



On the other hand, holes are trapped at PO₄³⁻ tetrahedra and form a phosphorous-oxygen-hole center (POHC).



Subsequently, holes trapped at POHC transfer to Ag⁺ and form Ag²⁺.



The processes of Ag₂⁺ (2) and Ag²⁺ (3) formation proceed with time at room temperature. As a result, the RPL intensity increases with time at room temperature. This effect is known as “build-up”.^(28,30,31) In addition, Ag⁰, Ag²⁺, and Ag₂⁺ can be eliminated by heating at 673 K for 1 h.^(26,32) Therefore, Ag-doped phosphate glasses have been used in reusable personal dosimeters. Although some RPL materials have been reported, the development of new RPL materials with RPL properties superior to those of Ag-doped phosphate glasses has not been achieved. To improve RPL materials, new RPL materials should be developed.

Considering the example of the Ag-doped phosphate glasses, materials wherein the silver valence changes and cluster formation occurs when energy is applied would be candidates of new Ag-doped RPL materials. In this study, we focused on Ag-doped Na–Al borate glass (BG:Ag) as such a material. It was previously reported⁽³³⁾ that luminescent silver clusters (Ag_3^+) were formed by irradiation with a femtosecond laser. In addition, the silver clusters were deleted by heating at 773 K for 1 h. Therefore, if a valence change or cluster formation of silver is induced by ionizing radiation, BG:Ag exhibits RPL, and BG:Ag is a candidate reusable RPL material. In this study, we aimed to develop a new Ag-doped RPL material and investigated the RPL properties and RPL center formation mechanism in BG:Ag.

2. Materials and Methods

$(100 - x)(30\text{Na}_2\text{O}-5\text{Al}_2\text{O}_3-65\text{B}_2\text{O}_5)-x\text{Ag}_2\text{O}$ ($x = 0$ and 1) glass samples were synthesized by the melt-quenching method in air. The raw materials Na_2CO_3 (99.9%; Rare Metallic Co. Ltd.), Al_2O_3 (99.99%; High Purity Chemicals Co., Ltd.), H_3BO_3 (99.99%; High Purity Chemicals Co., Ltd.), and Ag_2O (99.0%; Wako Pure Chemical Industries Ltd.) were mixed, loaded into an alumina crucible, and melted at 1373 K in an electric furnace (Barnsted International, 1300 Furnace model FB1314M). The liquid melt was poured onto a stainless-steel plate heated to 573 K and then the liquid melt was cooled to room temperature in air.

The glass samples were irradiated using an X-ray generator (Rigaku, RINT 2200) with a Cu X-ray tube operated at 40 mA and 40 kV. The samples were irradiated to 1–1000 Gy at the position where the dose rate was measured to be 1, 100, and 500 Gy/min using a reference dosimeter (RAMTEC Light, Toyo Medic).

First, to investigate the RPL properties, UV–Vis absorption, photoluminescence (PL), and electron spin resonance (ESR) spectra were measured at each dose. UV–Vis absorption spectra in the range of 200–800 nm were measured using a spectrometer (UV-2700, SHIMADZU). The excitation–emission mappings were measured in the unirradiated and 1-kGy-irradiated samples with an L42 optical filter (HOYA) in the excitation and emission wavelength ranges of 240–400 and 400–800 nm, respectively. In addition, the PL spectra with the excitation wavelengths of 320, 360, and 560 nm were measured with a spectrometer (F-7000, Hitachi). The ESR spectra were measured with a JES-X330 spectrometer (JEOL). Second, the variations of the PL and ESR spectra over time at ambient temperature (~ 298 K) were measured for 1 and 2 h immediately after 1 kGy of irradiation (500 Gy/min, 2 min) to investigate the RPL center formation mechanism, respectively. Finally, we measured the heating temperature dependences of PL and ESR spectra of BG:Ag after 1 kGy irradiation of X-rays (100 Gy/min, 10 min) to investigate the effect of heating on RPL properties. The irradiated samples were heated at 298, 373, 473, 573, 673, and 773 K with an electric furnace for 1 h. In addition, to investigate reusability, the PL spectra were measured in BG:Ag subjected to two cycles of heating and irradiation.

3. Results and Discussion

Figure 1 shows the absorption spectra and absorption difference spectra of the samples. In the nondoped borate glass sample (BG), the absorption band at 500–700 nm with the peak at 560 nm appeared after irradiation of ionizing radiation. On the basis of a previous report,⁽³⁴⁾ the absorption band with the peak at 560 nm is attributed to the boron oxygen hole center (BOHC). These results suggest that BOHC was formed by ionizing radiation in BG. On the other hand, a broad absorption band composed of two or more bands at 260–550 nm appeared in BG:Ag. In BG, no significant change in absorption at 260–500 nm was observed. Therefore, the broad absorption band at 260–500 nm can be attributed to Ag species. Although the optical absorption bands of Ag species have been investigated for a long time, the origin of absorption bands of silver species in various glasses is difficult and has not yet been established. According to a previous report,⁽³⁵⁾ absorption bands at 270, 310, and 340 nm are attributed to Ag_2^+ , Ag^{2+} , and Ag^0 in a Ag-doped Na–Al phosphate glass, respectively. Other researchers reported that the absorption band at 320 nm is attributed to Ag^{2+} or Ag_3^{2+} , and the band at 370 nm is attributed to

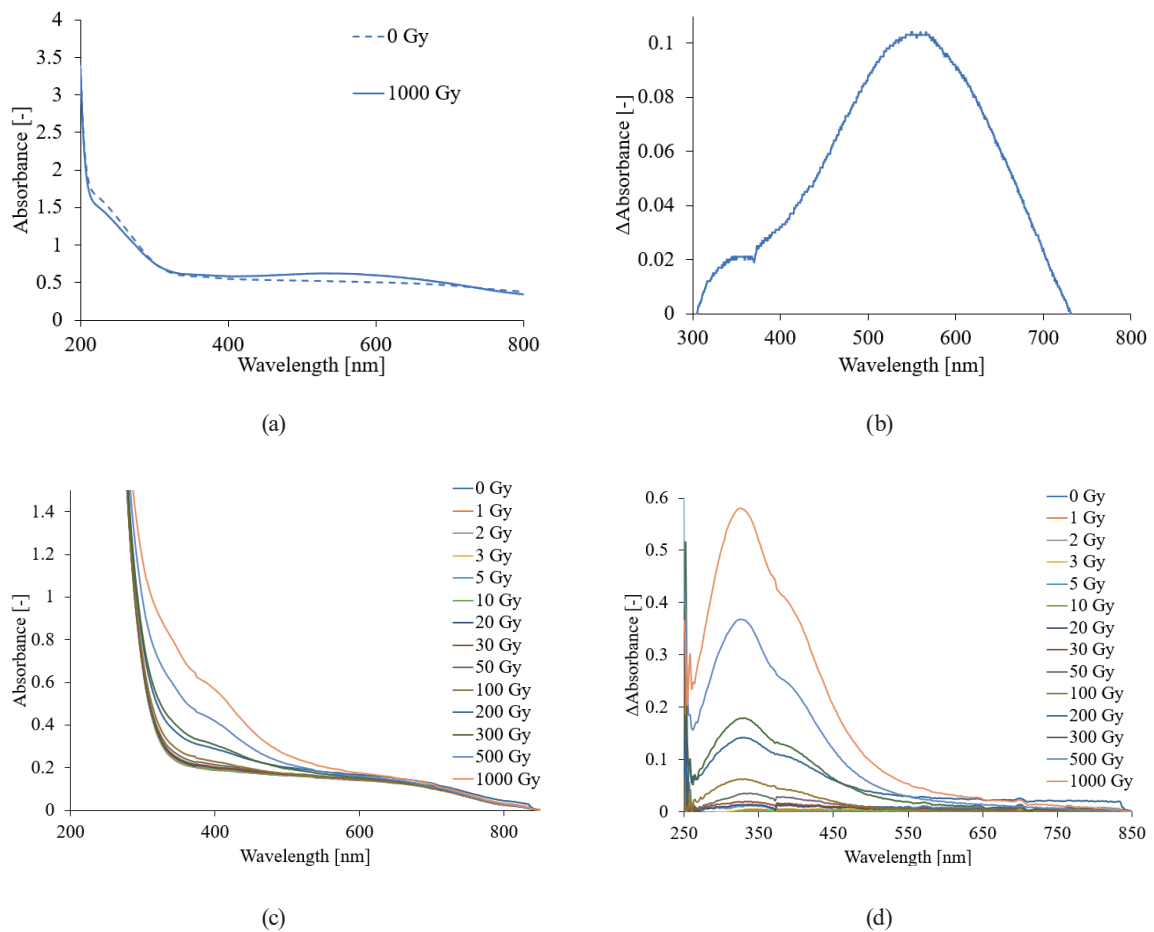


Fig. 1. (Color online) Absorption spectra and absorption difference spectra in (a), (b) BG and (c), (d) BG:Ag.

Ag^0 in Ag-doped Zn–Ga phosphate glass.⁽³⁶⁾ Although the origins of the absorption bands of Ag species have not yet been established, previous researchers reported the appearance of new absorption bands due to valence change and the clustering of Ag. These results indicate that valence change and the clustering of Ag were induced by ionizing radiation in BG:Ag.

Figure 2 shows the excitation–emission mapping of the difference in the luminescence intensity between unirradiated and 1-kGy-irradiated BG:Ag. Figure 2 also shows that a broad emission band at 450–800 nm was generated after the irradiation of ionizing radiation with the excitation wavelength range of 300–390 nm. The broad emission band seemed to have peaks at the excitation wavelengths of 320 and 360 nm. Therefore, we determined the excitation wavelengths to be 320 and 360 nm in BG:Ag.

Because the absorption band peak at 560 nm was generated after the irradiation of ionizing radiation in BG, emission spectra with an excitation wavelength of 560 nm were measured in addition to the excitation wavelengths of 320 and 360 nm. Figure 3 shows the emission spectra of BG. In all the spectra, no new emission band was observed after irradiation with X-rays. This result indicates that BG does not exhibit RPL.

Figure 4 shows the emission spectra of BG:Ag. New broad emission bands with the peak at approximately 650 nm appeared in both spectra after the irradiation of X-rays. According to a previous report,⁽²⁸⁾ in the case of Ag-doped phosphate glasses, the emission at 650 nm is attributed to Ag^{2+} and Ag_2^+ . These results suggest that BG:Ag exhibits RPL from Ag^{2+} and Ag_2^+ .

Figure 5 shows the dose dependence of the RPL intensity. With both excitation wavelengths, the RPL intensity increased linearly in the dose range of 1–300 Gy and became slightly saturated with a dose higher than 500 Gy. This saturation of PL intensity in the high dose range is considered as concentration quenching. On the basis of the 3σ method, detection limits with the excitation wavelengths of 320 and 360 nm were estimated to be approximately 20 and 5 Gy,

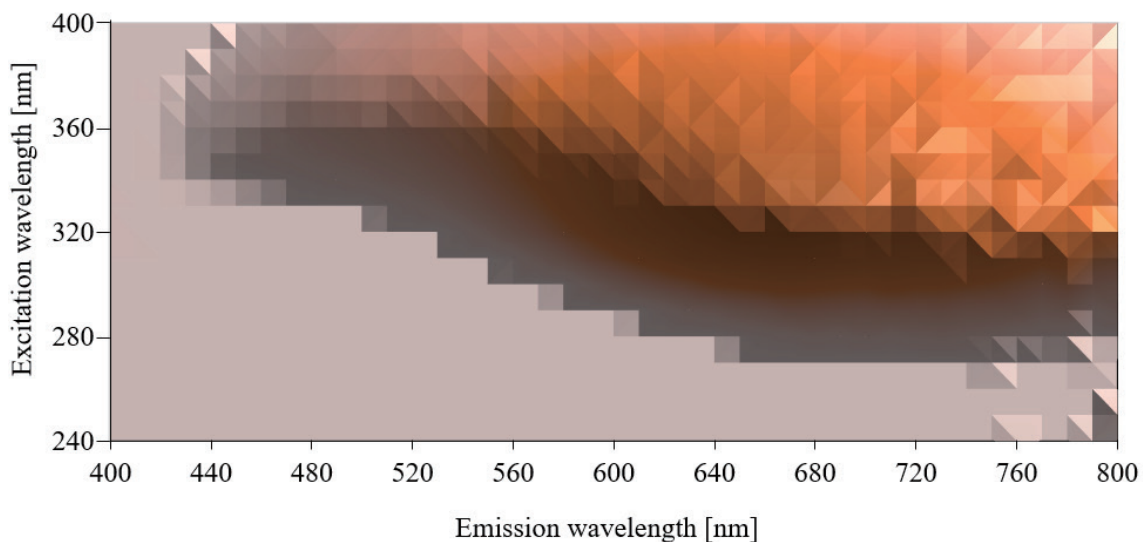


Fig. 2. (Color online) Excitation–emission mapping of the difference in luminescence intensity between unirradiated and 1-kGy-irradiated BG:Ag.

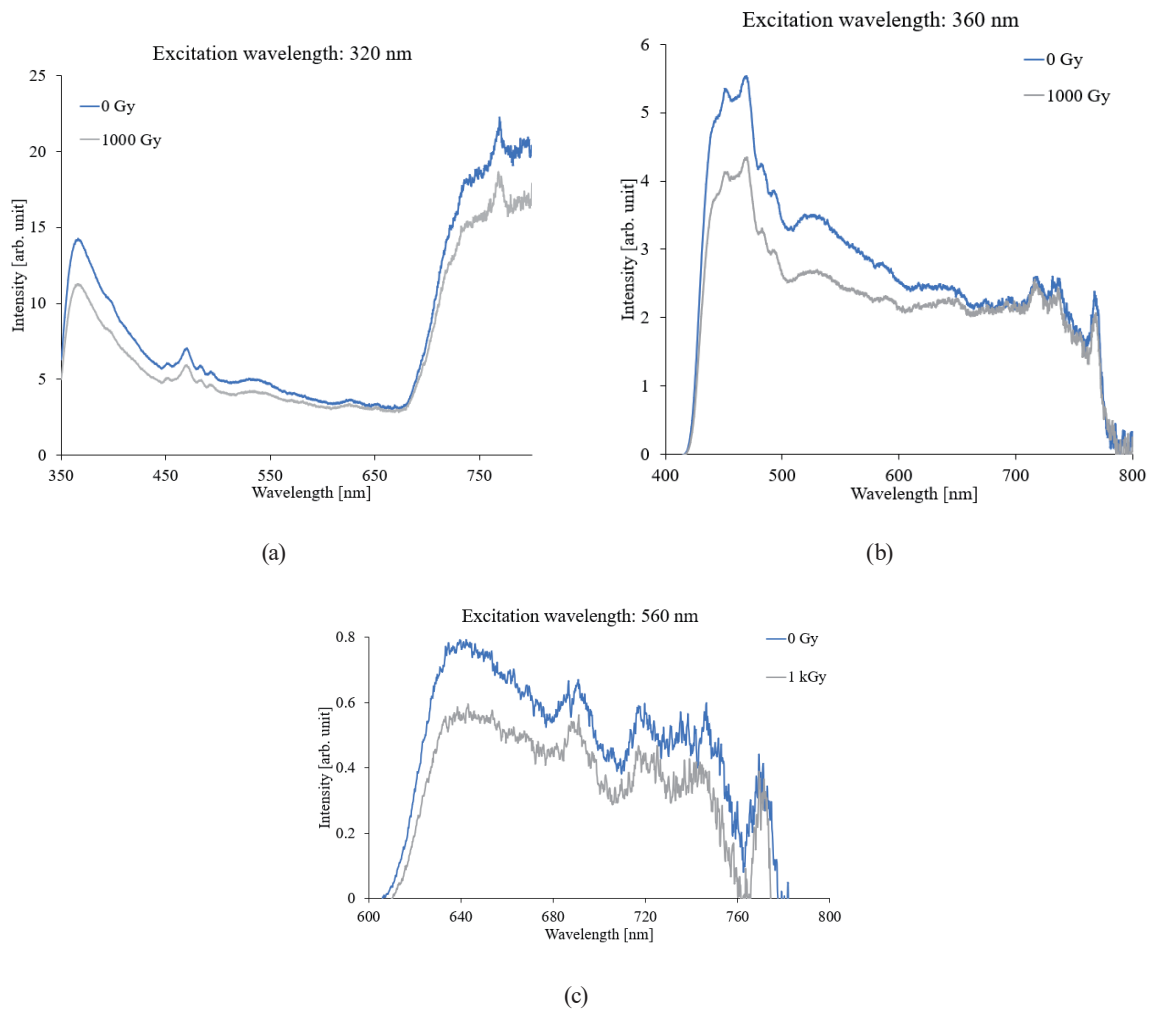


Fig. 3. (Color online) Emission spectra with excitation wavelengths of (a) 320, (b) 360, and (c) 560 nm in BG.

respectively. These results indicate that BG:Ag can be a candidate RPL dosimeter in the dose range of 5–300 Gy with the excitation wavelength of 360 nm.

Figure 6 shows the ESR spectra of the glass samples. In both glasses, the four-split signal was observed at 335 mT after irradiation. According to previous reports,^(34,37) this signal is attributed to BOHC. In the PL measurement result, BG did not exhibit RPL. These results indicate that BOHC does not act as an RPL center. In BG:Ag, the ESR signals were observed at approximately 310, 325, 335, and 370 mT after irradiation. The four-split signal at 335 mT is the same as the ESR signal observed in BG. Hence, the ESR signal of BOHC was generated by irradiation also in BG:Ag. On the basis of previous reports,^(28,32) the ESR signals at 310 and 370 mT are attributed to Ag_2^+ . On the other hand, the ESR signal at 325 mT is attributed to Ag^{2+} . These results indicate that in BOHC, Ag^{2+} and Ag_2^+ were formed by ionizing radiation in BG:Ag. As mentioned above, BOHC does not act as an RPL center. Therefore, Ag^{2+} and Ag_2^+ can be attributed to RPL centers in BG:Ag. Figure 7 shows the dose dependence of the ESR signal

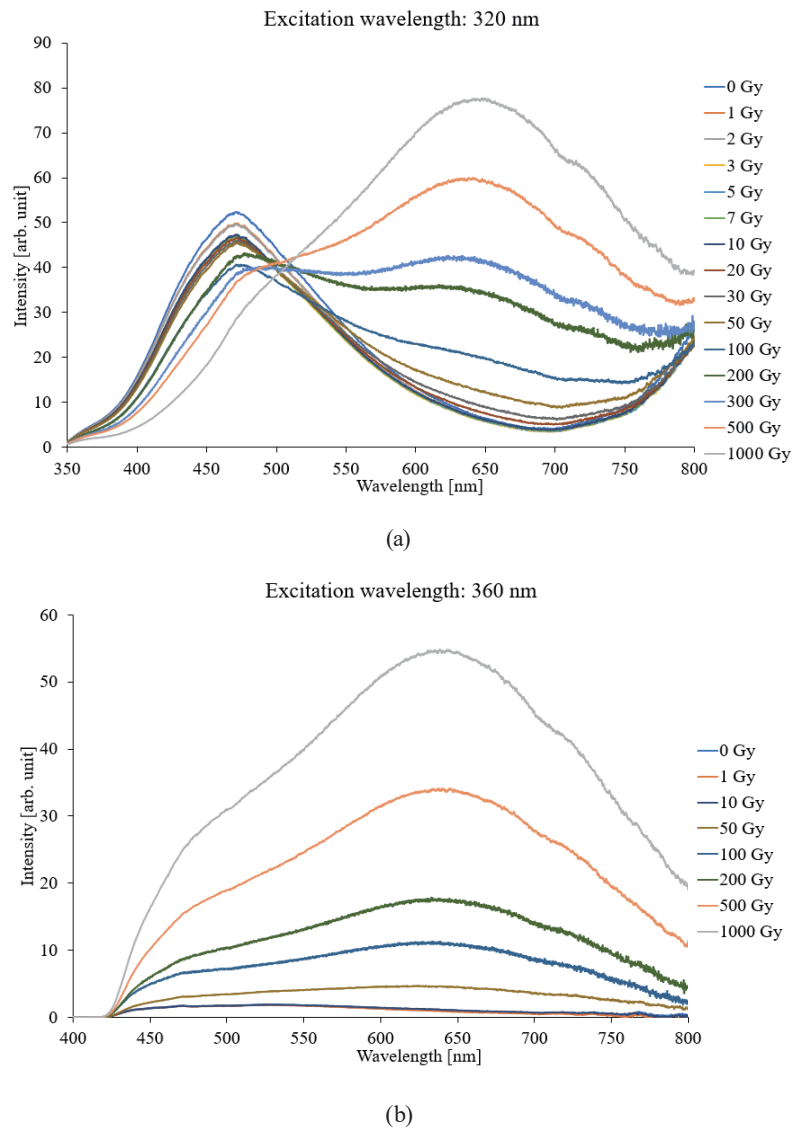


Fig. 4. (Color online) Emission spectra with excitation wavelengths of (a) 320 and (b) 360 nm in BG:Ag.

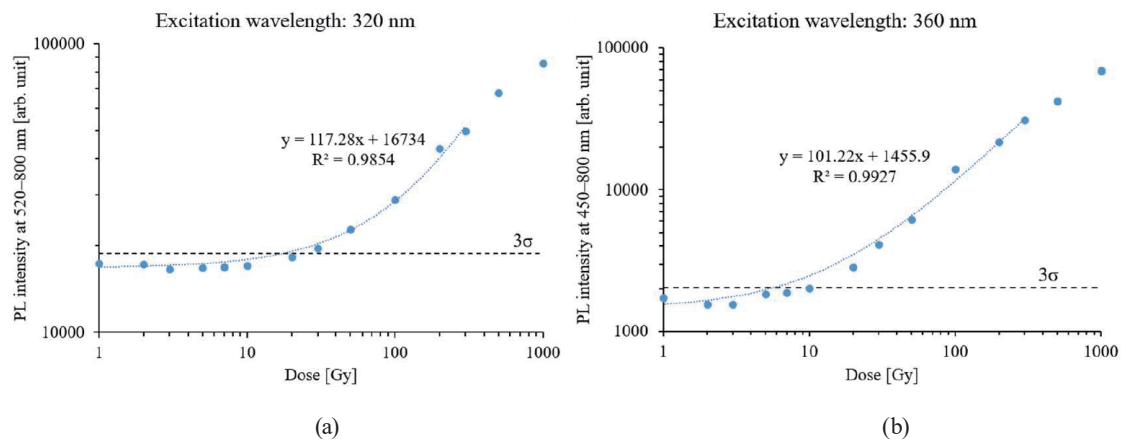


Fig. 5. (Color online) Dose dependences of RPL intensity with excitations at (a) 320 and (b) 360 nm. The dotted line indicates the 3σ value.

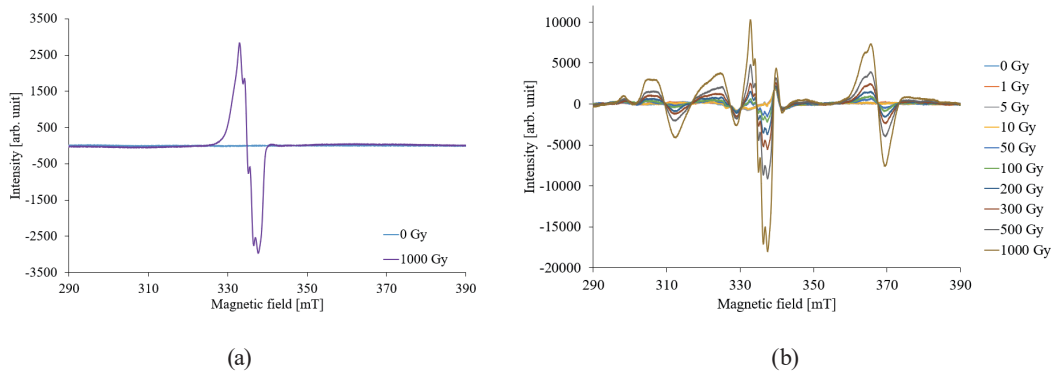


Fig. 6. (Color online) ESR spectra in (a) BG and (b) BG:Ag.

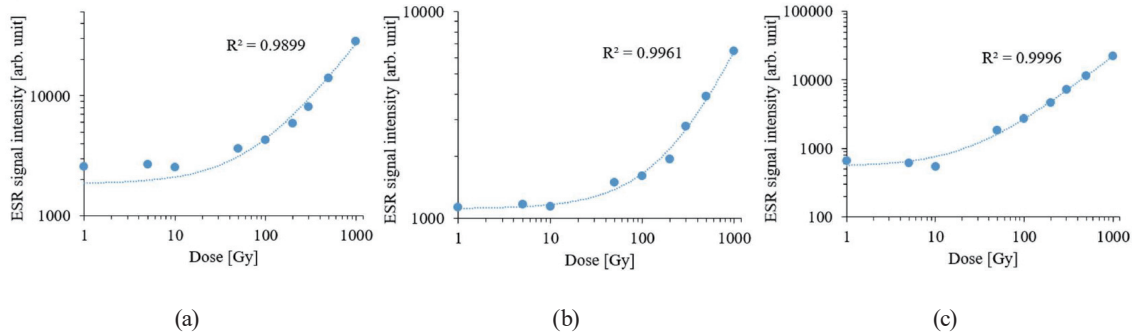


Fig. 7. (Color online) Dose dependences of ESR signals of (a) BOHC, (b) Ag_2^+ , and (c) Ag_2^+ in BG:Ag.

intensity. All of the ESR signal intensities corresponding to the formation yields of BOHC, Ag_2^+ , and Ag_2^+ increased linearly in the dose range of 1–1000 Gy. This result supports the concentration quenching of PL intensity in the high dose range.

Figure 8 shows the variation of the RPL spectra with time. In both spectra, the intensity at 400–800 nm increased with time. This increase in the RPL intensity is known as “build-up”, as mentioned in Sect. 1. These results indicate that the RPL center formation reaction proceeded with time at room temperature.

Figure 9 shows the time dependences of the RPL intensities at 650 nm. In the case of the excitation wavelength of 320 nm, the RPL intensity increased for 24 min and almost saturated after 26 min. On the other hand, in the case of the excitation wavelength of 360 nm, the RPL intensity increased continuously for 58 min. These results suggest that the different RPL centers were excited with different excitation wavelengths. In addition, the formation of the RPL center excited at 320 nm was completed in 24 min at room temperature.

Figure 10 shows the variations of the ESR spectra and ESR signal intensity with time. Shortly after irradiation, the doublet ESR signals at 300 and 370 mT and the four-split ESR signal of BOHC were observed. On the basis of a previous report,⁽³⁸⁾ the doublet ESR signals are attributed to Ag^0 . The doublet ESR signals of Ag^0 became broad ESR signals of Ag_2^+ . As shown in Figs. 10(b) and 10(c), the ESR signal intensity of BOHC decreased and the ESR signal

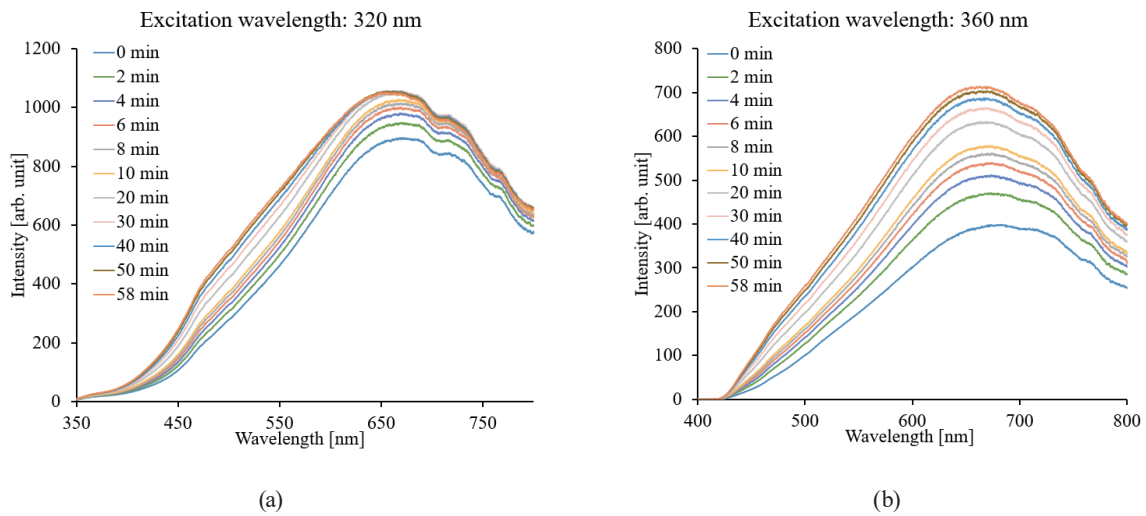


Fig. 8. (Color online) Variations in RPL spectra over time with excitations at (a) 320 and (b) 360 nm.

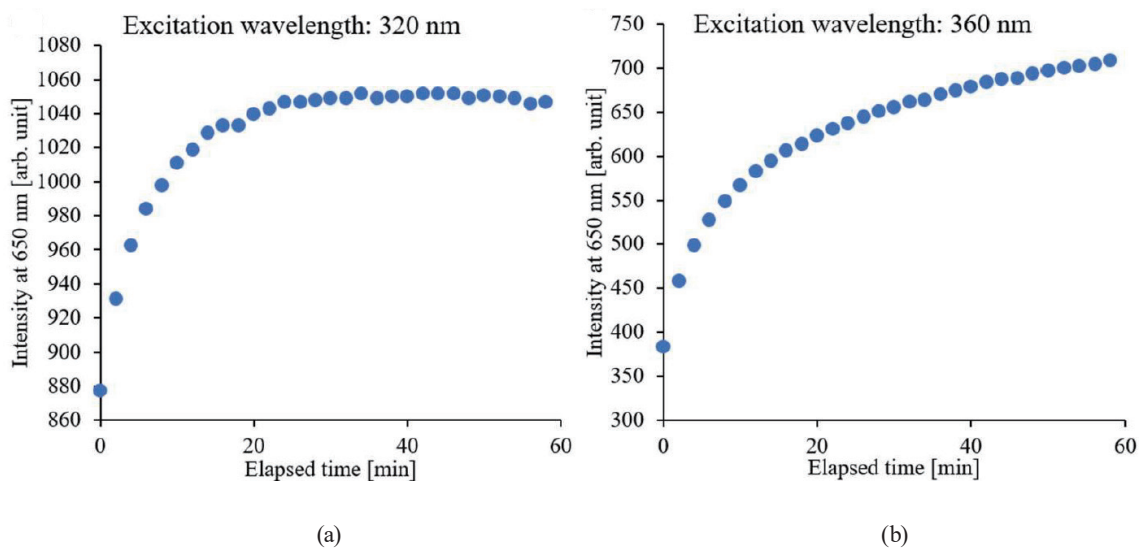


Fig. 9. (Color online) Time dependences of RPL intensity with excitations at (a) 320 and (b) 360 nm.

intensity of Ag^{2+} increased with time. These results indicate that Ag^{2+} and Ag_2^+ formation proceeded with time at room temperature. On the basis of the results of the variation of ESR spectra, we discuss the RPL center formation mechanism in BG:Ag. As mentioned above, the ESR signal intensities of BOHC and Ag^{2+} decreased and increased with time, respectively. In addition, the doublet ESR signal of Ag^0 changed into the broad ESR signal of Ag_2^+ . On the basis of these results, we assumed the following RPL center formation mechanism. First, electron–hole pairs are formed by ionizing radiation. Electrons are trapped at Ag^+ and form Ag^0 .



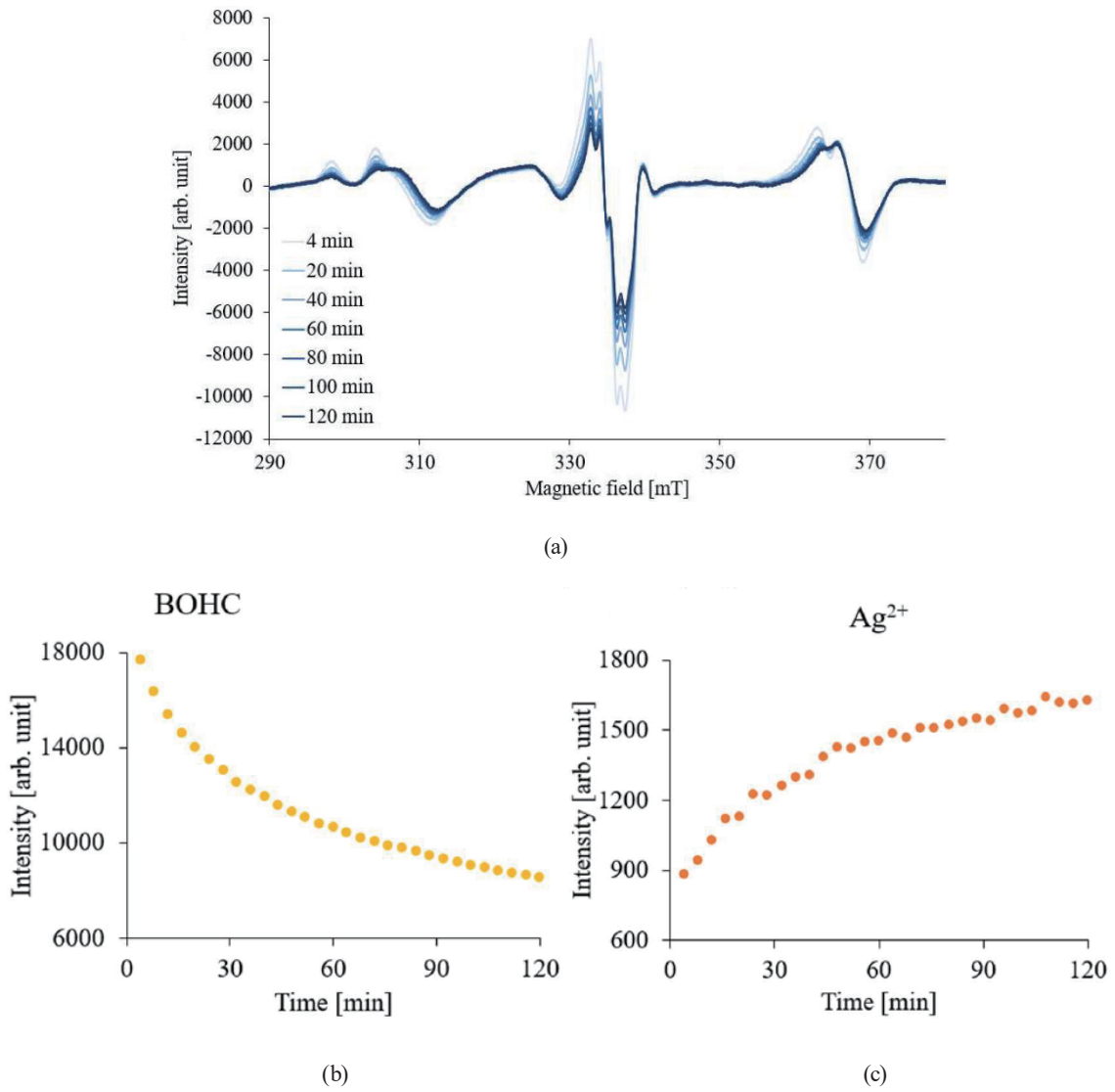


Fig. 10. (Color online) Variation of (a) ESR spectra and ESR signal intensities of (b) BOHC and (c) Ag^{2+} over time.

Subsequently, Ag_2^+ ions are formed by the association of Ag^+ and Ag^0 .



On the other hand, holes are trapped at the boron-oxide network and form BOHC.



Subsequently, holes trapped at BOHC transfer to Ag^+ and Ag^{2+} .



Figure 11 shows the temperature dependences of the PL spectra and PL intensity of 1-kGy-irradiated BG:Ag. At both excitation wavelengths, the PL intensity at 450–750 nm increased and decreased upon heating at 298–573 K and 573–773 K, respectively. After heating at 773 K, the PL intensity decreased to the same level as that of the unirradiated sample. These results revealed that the minimum temperature to eliminate RPL centers was 773 K.

Figure 12 shows the temperature dependences of the ESR spectra and ESR signal intensities of the 1-kGy-irradiated sample. The ESR signal intensities at 310, 370, and 335 mT, which are attributed to Ag_2^+ and Ag^{2+} , were decreased with increasing heating temperature. The decrease in the four-split ESR signal intensity of BOHC was observed in the temperature range of 298–473 K. Then, the singlet signal was clearly observed after heating at 573 K. The singlet signal intensity at 340 mT decreased after heating at 673–773 K. Finally, the ESR spectra became the same as that of the unirradiated sample after heating at 773 K. This result indicates that paramagnetic species generated by ionizing radiation were completely eliminated by heating at 773 K. To determine the origin of the singlet ESR signal, we focused on the hyperfine splitting

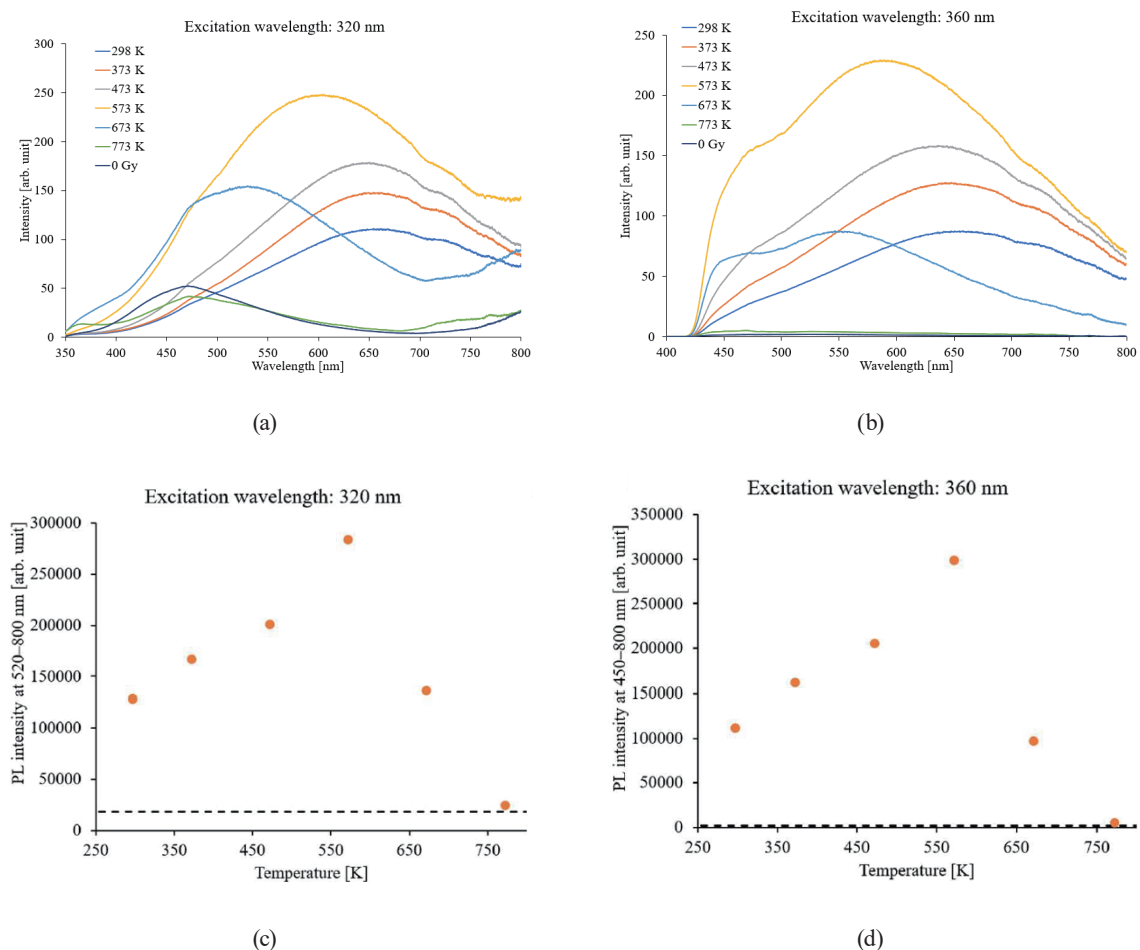


Fig. 11. (Color online) Heating temperature dependence of PL spectra and PL intensity with excitation wavelengths of (a), (c) 320 and (b), (d) 360 nm. The dotted line indicates the PL intensity of the unirradiated sample.

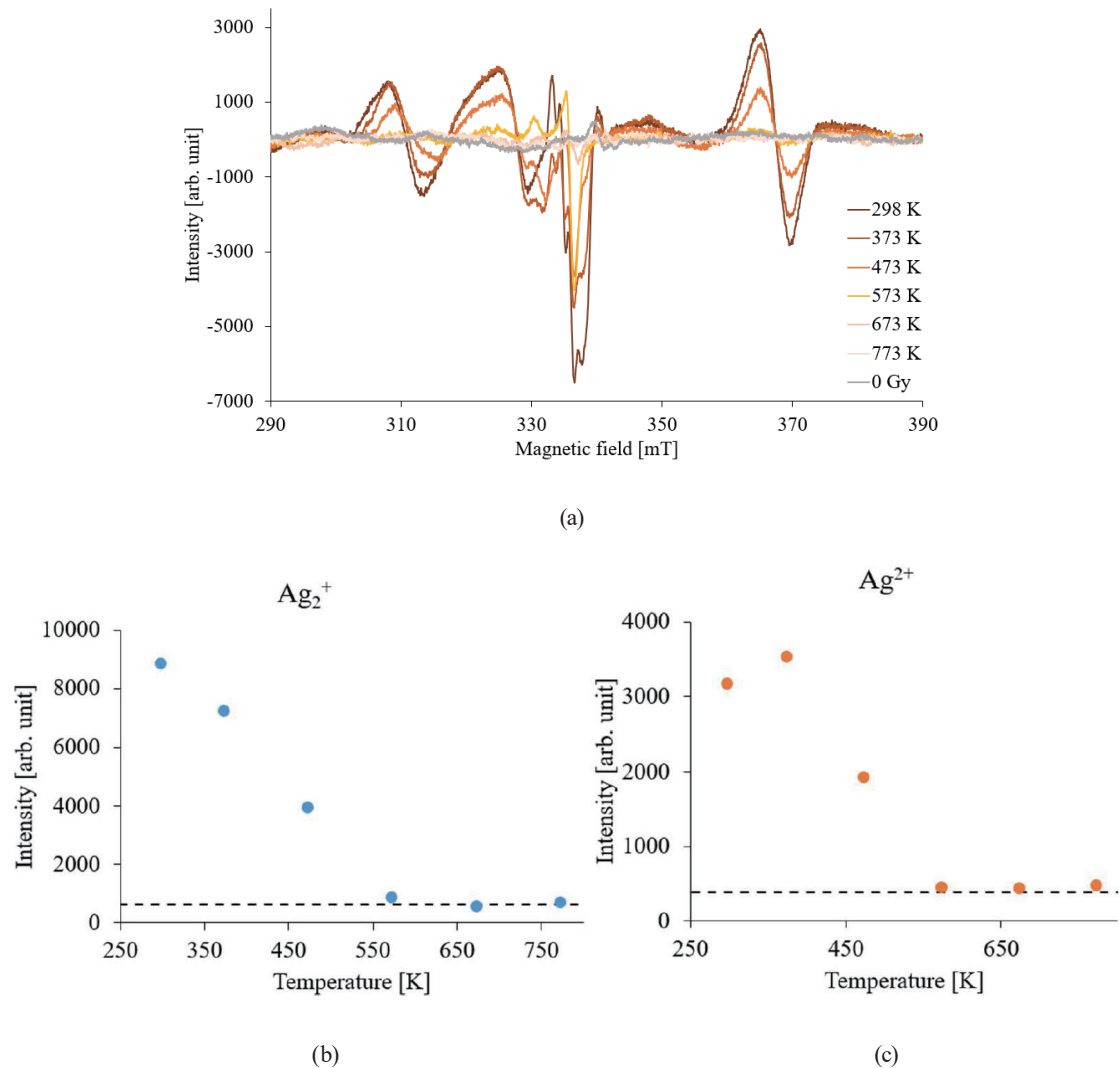


Fig. 12. (Color online) Heating temperature dependences of (a) ESR spectra and ESR signal intensities of (b) Ag_2^+ and (c) Ag^{2+} . The dotted lines indicate the ESR signal intensity of the unirradiated sample.

(hfs) of the ESR signal. Hfs is defined as splits in the energy levels caused by the interaction of the nuclear spin with the electron spin. If I is the nuclear spin of the nuclei interacting with electrons or holes, the number of hyperfine splittings n of the ESR signal can be expressed as $n = 2 * I + 1$. Hence, the singlet signal can be attributed to electron or hole nuclei with the nuclear spin of 0. In BG:Ag, the only nucleus with a nuclear spin of 0 is that of ^{16}O . Therefore, the singlet signal that appeared after heating at 573 K can be attributed to electrons or holes trapped at O-related centers. Figure 12(b) shows that the ESR signal intensity of Ag_2^+ monotonically decreased to the same level as that of the unirradiated sample upon heating at 298–573 K. In the temperature range of 573–773 K, no significant variation of the ESR signal intensity of Ag_2^+ was observed. These results indicate that Ag_2^+ was eliminated completely by heating at 573 K. Figure 12(c) shows that the ESR signal intensity of Ag^{2+} was increased by heating at 373 K. As

mentioned above, the ESR signal of BOHC decayed in the temperature range of 298–473 K. These results indicate that the Ag^{2+} formation reaction (4) was promoted by heating at 373 K. Subsequently, the Ag^{2+} signal intensity was decreased to almost the same level as that of the unirradiated sample by heating at 473–573 K. In 573–773 K, no significant variation of the ESR signal intensity of Ag^{2+} was observed. These results showed that Ag^{2+} was completely eliminated by heating at 773 K.

We now discuss the difference in the heating temperature dependences of PL and ESR signal intensities. PL intensities increased in the temperature range of 298–373 K. On the other hand, the ESR signal intensities of Ag^{2+} and Ag_2^+ decreased in the temperature range of 373–573 K. If the RPL centers in BG:Ag are only Ag^{2+} and Ag_2^+ , the PL intensities should decrease after heating at 373–573 K. However, the results were not so. The temperature dependence of the PL spectra shows that the emission peak wavelength seemed to shift to the short wavelength region. This result suggests that other luminescence centers were formed by heating after irradiation. In the ESR spectra, the singlet ESR signal of electrons or holes trapped at oxygen-related centers appeared after heating at 573 K. Hence, the oxygen-related paramagnetic species may act as the luminescence center. In addition, there is the possibility of the formation of new RPL centers without any unpaired electrons that are ESR-undetectable species. According to a previous study,⁽³³⁾ Ag_3^+ clusters are formed by irradiating a femtosecond laser into glass with the same composition as that of the glass sample used in this study. Furthermore, the formation of much larger Ag clusters in glass irradiated with ionizing radiation has been reported.^(39,40) Therefore, other luminescent Ag clusters undetectable by ESR might be formed by heating at 373–573 K after X-ray irradiation and function as RPL centers.

Figure 13 shows the RPL and ESR spectra of BG:Ag after heating. In Fig. 13, the RPL emission band was repeatedly eliminated by heating and generated by irradiation. This result indicates that BG:Ag is a candidate reusable RPL material.

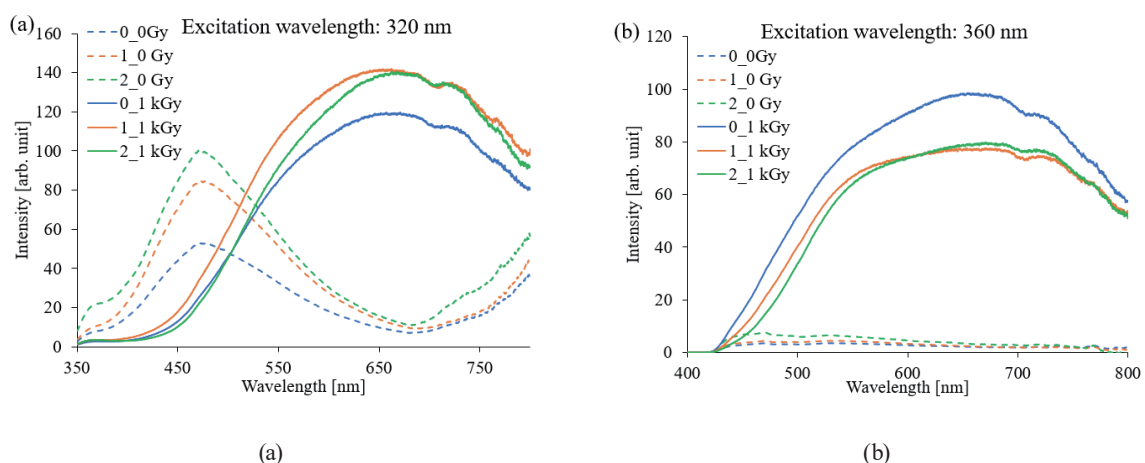


Fig. 13. (Color online) RPL spectra with excitations at (a) 320 and (b) 360 nm in BG:Ag after heating at 773 K for 1 h following irradiation. The unirradiated and 1-kGy-irradiated sample after n times of repeated heating is expressed as n_0 Gy and n_1 kGy in the legend, respectively.

4. Conclusions

In this study, we investigated the RPL properties and RPL center formation mechanism in Ag-doped Na–Al borate glass. Broad emission bands with the peak at 650 nm appeared after the irradiation of X-rays. Therefore, it was revealed that BG:Ag exhibits RPL. On the basis of the ESR measurements, Ag^{2+} and Ag_2^+ were attributed to the RPL centers in BG:Ag. In addition, these RPL centers could be deleted by heating at 773 K for 1 h and repeatedly regenerated by X-ray irradiation after being eliminated. These results indicate that BG:Ag is a candidate reusable RPL material. Finally, we elucidated the RPL center formation mechanism in BG:Ag on the basis of the variation of the ESR spectra with time immediately after irradiation. The proposed RPL center formation mechanism is as follows. First, electron–hole pairs are generated by ionizing radiation. Some of the electrons are trapped at Ag^+ and form Ag^0 . Subsequently, Ag_2^+ ions are formed by the association of Ag^+ and Ag^0 . On the other hand, holes are trapped at the boron-oxide network to form BOHC. Subsequently, the trapped holes transfer to Ag^+ from BOHC and form Ag^{2+} .

Acknowledgments

This work was supported by a Grant-in Aid for Scientific Research (A) (Grant No. 22H00308, 2022–2026) and a Grant-in-Aid for Scientific Research (B) (Grant No. 21H01853, 2021–2024) funded by the Japan Society for the Promotion of Science, the Kazuchika Okura Memorial Foundation 2022 research grant, and the Nakatani Foundation for the Advancement of Measuring Technologies in Biomedical Engineering 2022 General Research grant.

References

- 1 J. A. Perry: RPL Dosimetry: Radiophotoluminescence in Health Physics (Adam Hilger, Bristol, U.K., 1987) p. 3.
- 2 D. Y. C. Huang and S. M. Hsu: Advances in Center Therapy, H.G. Muhtasib Ed. (IN Tech, Rijeka, 2011) p. 553.
- 3 M. Martini and F. Meinardi: Thermally Stimulated Luminescence: New Perspectives in the Study of Defects in Solids (Riv. Nuovo Cim., 1997) p. 3.
- 4 C. Furetta and P. S. Weng: Operational Thermoluminescence Dosimetry (World Scientific Publishing, Singapore, 1998) p. 9.
- 5 L. Botter-Jensen, S. W. S. McKeever, and A. G. Wintle: Optically Stimulated Luminescence Dosimetry (Elsevier, Amsterdam, 2003) p. 1.
- 6 N. P. Patel, M. Srinivas, V. Verma, D. Modi, and K. V. R. Murthy: Adv. Mater. Lett. **7** (2016) 497. <https://doi.org/10.5185/amlett.2016.6160>
- 7 Y. Liu, Z. Chen, Y. Fan, W. Bs, W. Lu, Q. Guo, S. Pan, A. Chang, and X. Tang: Pro. Nat. Sci. **18** (2008) 1203. <https://doi.org/10.1016/j.pnsc.2008.04.002>
- 8 K. Nomura, T. Ikegami, and N. Juto: Radioisotopes **51** (2002) 85. <https://doi.org/10.3769/radioisotopes.51.85> (in Japanese).
- 9 S. Koyama, Y. Miyamoto, A. Fujiwara, H. Kobayashi, K. Ajisawa, H. Komori, Y. Takei, H. Nanto, T. Kurobori, H. Kakimoto, M. Sakakura, Y. Shimotsuma, K. Miura, K. Hirao, and T. Yamamoto: Sens. Mater. **22** (2010) 377. <https://doi.org/10.18494/SAM.2010.690>
- 10 M. Ranogajec-Komor, Knezevic, M., S. Z. Mijanac, and B. Vekic: Radiat. Meas. **43** (2008) 392. [https://doi.org/10.1016/j-radmeas.2007.11.020](https://doi.org/10.1016/j.radmeas.2007.11.020)
- 11 H. Nanto, Y. Miyamoto, T. Oono, Y. Takei, T. Kurobori and T. Yamamoto: Procedia Eng. **25** (2011) 231.
- 12 Z. Knezevic, N. Beck, D. Milkovic, S. Miljanic, and M. Ranogajec-Komor: Radiat. Meas. **46** (2011) 1582. <https://doi.org/10.1016/j.radmeas.2011.05.042>

- 13 T. Kurobori, and S. Nakamura: Radiat. Meas. **47** (2012) 1009. <https://doi.org/10.1016/j.radmeas.2012.09.003>
- 14 T. Kurobori, A. Takemura, Y. Miyamoto, D. Maki, Y. Koguchi, N. Takeuchi, T. Yamamoto, and Y. Q. Chen: Radiat. Meas. **83** (2015) 51. <https://doi.org/10.1016/j.radmeas.2015.04.017>
- 15 T. Kurobori, H. Itoi, Y. Yanagida and Y. Q. Chen: Nucl. Instrum. Methods Phys. Res A **793** (2015) 6. <https://doi.org/10.1016/j.nima.2015.04.062>
- 16 T. Kurobori, Y. Miyamoto, Y. Maruyama, T. Yamamoto and T. Sasaki: Nucl. Instrum. Methods Phys. Res. B. **326** (2014) 76. <https://doi.org/10.1016/j.nimb.2013.08.011>
- 17 T. Yanagida, G. Okada, T. Kato, D. Nakauchi, and N. Kawaguchi: Radiat. Meas. **158** (2022) 106847. <https://doi.org/10.1016/j.radmeas.2022.106847>
- 18 J. H. Schulman, R. J. Ginther, and C. C. Klick: J. Appl. Phys. **22** (1951) 1479. <https://doi.org/10.1063/1.1699896>
- 19 H. W. Etzel, J. H. Schulman, R. J. Ginther and E. W. Claffy: Phys. Rev. **85** (1952) 1063. <https://doi.org/10.1103/PhysRev.85.1063>
- 20 P. Boutinaud, A. Monnier, D. Lovy, and H. Bill: J. Phys. Chem. Solids **61** (2000) 1663. [https://doi.org/10.1016/S0022-3697\(00\)00023-8](https://doi.org/10.1016/S0022-3697(00)00023-8)
- 21 G. Okada, Y. Fujimoto, H. Tanaka, S. Kasap, and Y. Yanagida: J. Rare Earths **34** (2016) 769. [https://doi.org/10.1016/S1002-0721\(16\)60092-3](https://doi.org/10.1016/S1002-0721(16)60092-3)
- 22 G. Okada, W. Shinozaki, S. Ueno, Y. Koguchi, K. Hirasawa, F. D'Errico, F., T. Yanagida, S. Kasap, and H. Nanto: Jpn. J. Appl. Phys. **61** (2022) SB1035. <https://doi.org/10.35848/1347-4065/ac1ab2>
- 23 C. Pandey, S. M. Dhopte, and P. L. Muthal: Radiat. Eff. Defects Solids **162** (2007) 651. <https://doi.org/10.1080/10420150701197547>
- 24 R. L. Calvert, and R. J. Danby: Phys. Status Solidi **83** (1984) 597. <https://doi.org/10.1002/pssa.2210830222>
- 25 T. Kato, D. Nakauchi, N. Kawaguchi, and T. Yanagida: Mater. Lett. **270** (2020) 127688. <https://doi.org/10.1016/j.matlet.2020.127688>
- 26 H. Kawamoto, M. Koshimizu, Y. Fujimoto, and K. Asai: Jpn. J. Appl. Phys. **62** (2023) 010501. <https://doi.org/10.35848/1347-4065/ac9cb0>
- 27 Y. Miyamoto, T. Yamamoto, K. Kinoshita, S. Koyama, Y. Takei, H. Nanto, Y. Shimotsuma, M. Sakakura, K. Miura, and K. Hirao: Radiat. Meas. **45** (2010) 546. <https://doi.org/10.1016/j.radmeas.2010.01.012>
- 28 S. W. S. McKeever, S. Sholom, and N. Shrestha: Radiat. Meas. **123** (2019) 13. <https://doi.org/10.1016/j.radmeas.2019.02.009>
- 29 S. Sholom, and S. W. S. McKeever: Radiat. Meas. **163** (2023) 106924. <https://doi.org/10.1016/j.radmeas.2023.106924>
- 30 R. Yokota, and H. Imagawa: J. Phys. Soc. Jpn. **23** (1967) 1038. <https://doi.org/10.1143/JPSJ.23.1038>
- 31 H. Kawamoto, H. Tanaka, M. Koshimizu, Y. Fujimoto, and K. Asai: Nucl. Instrum. Methods Phys. Res. B **479** (2020) 137. <https://doi.org/10.1016/j.nimb.2020.06.014>
- 32 H. Kawamoto, I. Kawamura, H. Komiya, M. Koshimizu, Y. Fujimoto, and K. Asai: Jpn. J. Appl. Phys. **61** (2022) SB1026. <https://doi.org/10.35848/1347-4065/ac2626>
- 33 A. S. Lipatiev, S. S. Fedotov, S. V. Lotarev, T. O. Lipateva, G. Y. Shakhgildyan, and V. N. Sigaev: ACS Appl. Nano Mater. **5** (2022) 6750. <https://doi.org/10.1021/acsanm.2c00765>
- 34 P. Rautiyal, G. Gupta, R. Edge, L. Leay, A. Daubney, M. K. Patel, A.H. Jones, and P. A. Bingham: J. Nucl. Mater. **544** (2021) 152702. <https://doi.org/10.1016/j.jnucmat.2020.152702>
- 35 T. Kurobori, W. Zheng, Y. Miyamoto, H. Nanto, and T. Yamamoto: Opt. Mater. **32**, **9** (2010) 1231. <https://doi.org/10.1016/j.optmat.2010.04.004>
- 36 K. Bourhis, A. Royon, G. Papon, M. Bellec, Y. Petit, L. Canioni, M. Dussauze, V. Rodriguez, L. Binet, D. Caurant, M. Treguer, J. J. Videau, and T. Cardinal: Mater. Res. Bull. **48** (2013) 1637. <https://doi.org/10.1016/j.materresbull.2013.01.003>
- 37 T. Kishii and K. Ooka, J. Phys. Soc. Jpn. **23** (1967) 659. <https://doi.org/10.1143/JPSJ.23.659>
- 38 N. I. Mel'nikov, D. P. Peregood, and R. A. Zhitnikov, J. Non-Cryst. Solids **16** (1974) 195. [https://doi.org/10.1016/0022-3093\(74\)90124-0](https://doi.org/10.1016/0022-3093(74)90124-0)
- 39 C. Maurel, T. Cardinal, M. Bellec, L. Canioni, B. Bousquet, M. Treguer, J.J. Videau, J. Choi, M. Richardson: J. Lumin. **129** (2009) 1514. <https://doi.org/10.1016/j.jlumin.2008.12.023>
- 40 J. Harb, T. Guérineau, A. Morana, A. Meyer, G. Raffy, A. D. Guerso, Y. Ouerdane, A. Boukenter, S. Girard, T. Cardinal, Y. Petit, and L. Canioni: Chemosensors **10** (2022) 110. <https://doi.org/10.3390/chemosensors10030110>